Adaptive Model Parameter Estimation Triggered by the Beneficial Observation Rate from Forecast Sensitivity to Observations

Takumi Honda[a] and Yohei Sawada[b]

[a] *Information Technology Center, The University of Tokyo, Kashiwa, Chiba, Japan*

[b] *Graduate School of Engineering, The University of Tokyo, Tokyo, Japan*

Corresponding author: Takumi Honda, honda.takumi2024@mail.u-tokyo.ac.jp

ABSTRACT

In NWP, the assimilation of various observations contributes to improving forecast accuracy. The contribution of each observation can be estimated by existing methods. Empirically, it is well known that only a fraction of assimilated observations are diagnosed as beneficial, meaning that they improve forecast accuracy. Previous studies have indicated that the beneficial observation rate depends on model imperfections. Building on this sensitivity, we propose a new method that uses the beneficial observation rate to trigger adaptive model parameter estimation for mitigating model errors and bias. Specifically, the method activates model parameter estimation when the beneficial observation rate exceeds a prescribed threshold. Using the Lorenz96 40-variable system, we demonstrate that the new approach successfully detects model bias and improves analysis accuracy, even when the true model parameter varies in time. Furthermore, we find that the beneficial observation rate is useful for detecting model bias even when the model and observations have similar biases, in which case the time-averaged observation-minus-background does not provide a clear signal of the bias.

SIGNIFICANCE STATEMENT

In weather forecasting, many observations are combined with model forecasts to estimate the initial conditions for the next forecast. However, only some observations actually help improve forecast accuracy. Building on the fact that the proportion of beneficial observations is sensitive to model imperfections, we propose a new method that uses this rate to detect model imperfections and correct them. Using a low-dimensional system, we demonstrate that the proposed method can improve the estimated initial conditions. Future research should test the proposed method in a realistic weather forecasting system.

1. Introduction

In numerical weather prediction (NWP), data assimilation (DA) plays an important role in producing improved initial conditions. Specifically, DA combines various observations and model forecasts based on their uncertainties to obtain the best estimate of the current atmospheric state and thereby helps reduce forecast errors. Although DA generally estimates model state variables such as wind and temperature, it can also estimate uncertain model parameters such as empirical coefficients in parameterization schemes. Several studies have

successfully estimated various model parameters and mitigated detrimental impacts of model imperfections including model errors and bias (e.g., Anderson 2001; Aksoy et al. 2006a,b; Jung et al. 2010; Ruiz et al. 2013a,b; Schirber et al. 2013; Kotsuki et al. 2018, 2020; Nystrom et al. 2021, 2023; Sueki et al. 2022). Despite these successes, stably estimating model parameters remains challenging. Given discrepancies between observations and simulations, it is not straightforward to determine whether these differences arise from errors in model parameters or in state variables (Sawada and Duc 2024; Ruiz et al. 2013a,b). In other words, it is desirable to identify errors caused by model imperfections and determine when parameter estimation is needed.

In operational atmospheric DA systems, observations are routinely collected from various observing systems such as upper-air soundings, ships, buoys, aircraft, surface stations, weather radars, and satellites. The contribution of each observation to forecast error reduction, referred to as forecast sensitivity to observations (FSO), can be estimated using variational (Langland and Baker 2004) and ensemble-based methods (Kalnay et al. 2012). These methods have been widely used to identify beneficial (detrimental) observations that improve (degrade) forecast accuracy (e.g., Ota et al. 2013; Sommer and Weissmann 2014; Hotta et al. 2017; Ishibashi 2018; Chen and Kalnay 2020; Yamazaki et al. 2021; Privé et al. 2021; Yamazaki et al. 2023; Gasperoni et al. 2024; Honda et al. 2026).

It is well known that only a fraction of observations are diagnosed as beneficial. The proportion of beneficial observations among all observations, hereafter referred to as the beneficial observation rate, is typically 50–60% in practice (Lorenc and Marriott 2014; Hotta et al. 2017; Bormann et al. 2019; Samrat et al. 2025). Using a toy system, Lorenc and Marriott (2014) demonstrated that this moderate beneficial observation rate is associated with several factors such as the coexistence of decaying and growing modes, observation errors, errors in the reference used to evaluate forecast accuracy, and imperfect specification of background error covariance. Consistent with this, Kotsuki et al. (2019) and Privé et al. (2021) showed that self-analysis verification overestimates FSO in atmospheric DA systems. Kotsuki et al. (2019) also demonstrated that this overestimation can be mitigated to some extent by using the observation-based metric proposed by Sommer and Weissmann (2016).

Model imperfections also affect the beneficial observation rate (Lorenc and Marriott 2014; Dahoui et al. 2017). Necker et al. (2018) found that the FSO impacts of observations that correct model bias are overestimated. Privé et al. (2021) pointed out that the beneficial

impacts of observations rapidly decrease as the forecast lead time increases in the presence of model bias. These effects of model imperfections on the beneficial observation rate suggest that this metric may be useful for detecting model imperfections. However, despite these findings, it remains unclear whether the beneficial observation rate can be used as a practical indicator of model imperfections and incorporated into a model parameter estimation framework.

This study proposes a new FSO-based parameter estimation approach that exploits the sensitivity of the beneficial observation rate to model imperfections. In this approach, we use the beneficial observation rate obtained from FSO as a proxy for model imperfections, and parameter estimation is activated when the rate exceeds a prescribed threshold. We use the Lorenz96 40-variable system (Lorenz and Emanuel 1998), a widely used DA testbed, to investigate the sensitivity of the beneficial observation rate to model imperfections and evaluate the performance of the proposed approach. As shown later, the proposed approach can detect model imperfections and facilitate their correction through parameter estimation in the Lorenz96 40-variable system.

The remainder of this article is structured as follows. Section 2 describes the methodology for the Lorenz96 40-variable system experiments, and Section 3 presents the results and discussion. Finally, Section 4 summarizes the findings and provides concluding remarks.

2. Methodology

a. Lorenz96 40-variable model

1) MODEL EQUATION

This study uses the 40-variable model from Lorenz and Emanuel (1998), which has been extensively used as a testbed for various data assimilation studies (e.g., Miyoshi 2005; Kotsuki et al. 2017; Kurosawa and Poterjoy 2021; Tomizawa and Sawada 2021; Honda and Yamazaki 2024). The governing equation of the model is

$$\frac{dx_j}{dt} = (x_{j+1} - x_{j-2})x_{j-1} - x_j + F, \qquad (1)$$

where j denotes the grid index ($j = 0,1, \ldots ,39$), x_j is the state variable at the j-th grid point, t is the time, and F is the forcing term. F characterizes the behavior of the dynamical system. As F increases, the system behavior becomes more chaotic. As in previous studies, we set

$F = 8.0$ as the default value. According to Lorenz and Emanuel (1998), $F = 8.0$ produces chaotic system behavior and a non-dimensional time interval of 0.05 corresponds to 6 h in the real atmosphere based on forecast error growth. Periodic boundary conditions are applied. As in Chen and Kalnay (2019), the model is integrated with a non-dimensional time interval of 0.05 using the 4th-order Runge-Kutta method.

2) NATURE RUNS AND SYNTHETIC OBSERVATIONS

We perform two nature runs for observing-system simulation experiments (OSSEs). The first nature run is the baseline and uses a globally constant forcing term with $F = 8.0$, whereas the second nature run uses a time-varying forcing term at grid points with j between 20 and 24. In the second nature run, the forcing term is varied in time as $F(t) = 8.0 + F_{amp}\cos\left(2\pi t_{step}/t_{period}\right)$, where F_{amp} is the amplitude (=2.0), t_{step} is the number of time steps, and t_{period} is the period. t_{period} is set to $4 \times 365 \times 5 = 7{,}300$ time steps, which corresponds to 5 years in the dynamical model.

The initial conditions for the nature runs are set following previous studies (e.g., Honda and Yamazaki 2024). Specifically, we use initial conditions of $x = 8.0$ at all grid points, except at one grid point, where $x = 8.01$. We integrate the model for 200,500 time steps. Synthetic observations are generated by adding Gaussian noise, $N(0.0,1.0)$, to the state variables of the nature runs. For simplicity, we assume that the state variables are directly observed at every time step and every grid point.

b. Data assimilation

1) STATE ESTIMATION

We use the local ensemble transform Kalman filter (LETKF, Hunt et al. 2007), a variant of the ensemble Kalman filter (EnKF, Evensen 1994; Houtekamer and Zhang 2016), as the DA method. Our implementation of LETKF follows Miyoshi and Yamane (2007) and Miyoshi et al. (2007), in which state variables are locally updated at each grid point using observations close to the target grid point. Specifically, to estimate state variables at each grid point, observations within a distance of $2\sqrt{10/3}\,\sigma_{\mathrm{h}}$ are used, where σ_{h} is the horizontal localization scale. Observation errors are inflated as the distance increases using the Gaspari and Cohn (1999) function. To maintain a sufficient amount of ensemble spread, we employ a

simple multiplicative covariance inflation with coefficient ρ. We test various combinations of σ_{h} (0.5–10.0) and ρ (1.00–1.20) in Section 3a.

In each experiment with a different combination of σ_{h} and ρ, we perform 20,000 DA cycles starting from the time step of 100,000. We prepare the ensemble initial conditions by randomly sampling states from the nature runs at time steps between 50,000 and 90,000. Throughout this study, the ensemble size is fixed at 40.

2) ENSEMBLE FORECAST SENSITIVITY TO OBSERVATIONS (EFSO)

This study uses the ensemble-based FSO (EFSO) formulation derived by Kalnay et al. (2012). FSO measures the forecast error reduction at verification time t due to the assimilation of observations at time 0. Forecast errors are calculated against a reference state $\mathbf{x}_{ref}$ as follows:

	$\mathbf{e}_{t\|0} = \mathbf{x}_{t\|0} - \mathbf{x}_{ref},$	
	$\mathbf{e}_{t\|-1} = \mathbf{x}_{t\|-1} - \mathbf{x}_{ref},$	

where $\mathbf{x}_{t|0}$ and $\mathbf{x}_{t|-1}$ denote the forecast states valid at time t, initiated at times 0 and -1, respectively. Here, the time interval of DA cycles is assumed to be 1. Time t represents the lead time of the EFSO evaluation forecast. In this study, unless otherwise stated, the EFSO evaluation forecast lead time is set to 1 time step and observations are used as reference states. Using the error norm $\mathbf{C}$, the forecast error reduction is calculated as follows:

	$\Delta\mathbf{e}^2 = \mathbf{e}_{t\|0}^T\mathbf{C}\mathbf{e}_{t\|0} - \mathbf{e}_{t\|-1}^T\mathbf{C}\mathbf{e}_{t\|-1},$	
	$= \left(\mathbf{e}_{t\|0} - \mathbf{e}_{t\|-1}\right)^T\mathbf{C}\left(\mathbf{e}_{t\|0} + \mathbf{e}_{t\|-1}\right),$	

Using the forecast model's Jacobian $\mathbf{M}$, the Kalman gain $\mathbf{K}$, and the innovation vector $\delta\mathbf{y}_0$, this equation can be approximated as:

	$\Delta\mathbf{e}^2 \approx [\mathbf{M}(\mathbf{K}\delta\mathbf{y}_0)]^T\mathbf{C}\left(\mathbf{e}_{t\|0} + \mathbf{e}_{t\|-1}\right).$	

Substituting $\mathbf{K} = \mathbf{A}\mathbf{H}^T\mathbf{R}^{-1} = [1/(K-1)]\mathbf{X}_a(\mathbf{X}_a)^T\mathbf{R}^{-1}$, where $\mathbf{A}$ is the analysis error covariance matrix, $\mathbf{H}$ is the Jacobian of the observation operator, $\mathbf{R}$ is the observation error covariance matrix, and K is the ensemble size, yields

	$\Delta\mathbf{e}^2 \approx \left[\mathbf{M}\left(\frac{1}{K-1}\mathbf{X}_a(\mathbf{X}_a)^T\mathbf{H}^T\mathbf{R}^{-1}\delta\mathbf{y}_0\right)\right]^T\mathbf{C}\left(\mathbf{e}_{t\|0} + \mathbf{e}_{t\|-1}\right),$	

	$= \left[\frac{1}{K-1}\mathbf{X}_f(\mathbf{X}_a)^T\mathbf{H}^T\mathbf{R}^{-1}\delta\mathbf{y}_0\right]^T \mathbf{C}\left(\mathbf{e}_{t\|0} + \mathbf{e}_{t\|-1}\right),$	
	$\approx \frac{\delta\mathbf{y}_0^T}{K-1}\mathbf{R}^{-1}(\mathbf{Y}_a)^T\mathbf{X}_f^T\mathbf{C}\left(\mathbf{e}_{t\|0} + \mathbf{e}_{t\|-1}\right),$	

where $\mathbf{Y}_a$ denotes the analysis ensemble perturbations in the observation space and $\mathbf{X}_f$ denotes the forecast ensemble perturbations. The l-th element of $\Delta\mathbf{e}^2$ corresponds to the contribution (i.e., EFSO impact) of the l-th observation. As in Hotta et al. (2017), observations with negative EFSO impacts are referred to as beneficial. Given samples of EFSO impacts at each grid point from DA cycles, the beneficial observation rate is calculated as the proportion of negative (beneficial) EFSO impacts among the samples. In this study, as in Chen and Kalnay (2019), the error norm is set to the identity matrix. The spatial localization for EFSO is applied as in LETKF.

3) PARAMETER ESTIMATION USING EFSO

This study estimates not only the state variables but also the model parameter (F). We use the state augmentation method that extends the state vector to include model parameters (Anderson 2001; Aksoy et al. 2006b,a; Ruiz et al. 2013a). This enables simultaneous estimation of both the state variables and model parameters, provided that perturbations in model parameters result in a detectable response in observations (Nystrom et al. 2021, 2023). As Eq. (1) indicates, F affects the local tendency at each grid point. Therefore, for parameter estimation, we use a tight localization scale of 1.0. The covariance inflation coefficient for parameter estimation is set to 1.02. We perform a total of 20,000 DA cycles. As spin-up, we do not activate parameter estimation in the first 2,000 cycles.

The proposed new approach uses the beneficial observation rate from EFSO to trigger parameter estimation. Specifically, after spin-up, the beneficial observation rate at each grid point is calculated using EFSO against observations over the previous 400 DA cycles, which is larger than the sample size suggested by Lorenc and Marriott (2014). If the beneficial observation rate exceeds a threshold value, random ensemble perturbations sampled from $N(0.0,0.1^2)$ are added to F at the grid points where the beneficial observation rate exceeds the threshold value and at the neighboring grid points. At these grid points, parameter estimation is activated, whereas at the other grid points the ensemble spread of F remains zero and no parameter estimation is performed. If the beneficial observation rate falls below

184 the threshold value, the value of F is set to the ensemble mean in all ensemble members and
185 parameter estimation is deactivated.

186 For comparison with the proposed EFSO-based approach, we also perform additional
187 experiments in which parameter estimation is conducted without using EFSO. In these cases,
188 parameter estimation is activated by adding random perturbations from $N(0.0,0.1^2)$ at all grid
189 points after the first 2,000 DA cycles, regardless of the beneficial observation rate.

190 *c. Model and observation biases in each case*

191 We consider a total of eight cases (Table 1). Cases 1–3 use the baseline nature run. In
192 these cases, the true forcing term F is globally constant at 8.0. Case 1 uses the perfect model
193 for the DA system, in which F is identical to that in the first nature run, without parameter
194 estimation (hereafter NatureConst-Perfect-NoPE). Case 2 is the same as Case 1, except that it
195 assumes a spatially varying model bias in the DA system (hereafter NatureConst-Biased-
196 NoPE). Specifically, the DA system uses an imperfect model in which F is set to 10.0 for j
197 between 20 and 24, and to 8.0 elsewhere. Case 3 is the same as NatureConst-Biased-NoPE,
198 except that parameter estimation is performed with the new approach (hereafter NatureConst-
199 Biased-PE). Case 4 is the same as NatureConst-Biased-PE, except that parameter estimation
200 is activated without the new approach (i.e., regardless of the EFSO results) (hereafter
201 NatureConst-Biased-PE-NoEFSO).

202 Cases 5–7 use the second nature run, in which F varies in time. Case 5 does not perform
203 parameter estimation (hereafter NatureVary-Biased-NoPE). Cases 6 and 7 perform parameter
204 estimation with EFSO (new approach) and without EFSO, respectively (hereafter
205 NatureVary-Biased-PE and NatureVary-Biased-PE-NoEFSO). Case 8 uses the baseline
206 nature run and the imperfect model as in NatureConst-Biased-PE, but includes observation
207 bias for j between 20 and 24 (hereafter NatureConst-Biased-ObsBias-PE).

208 Strictly speaking, differences in F between the nature runs and the model used for a DA
209 system are model errors rather than model bias. In practice, however, increasing the value of
210 F results in a larger value of the state variables (Eq. (1)), corresponding to model bias.
211 Therefore, for simplicity, we refer to differences in F as model bias throughout this article.

Case number	Case name	Nature run	Model used for the DA system	Observation bias	Parameter estimation (PE)
1	NatureConst-Perfect-NoPE	Baseline (globally constant $F = 8.0$)	Perfect model (globally constant $F = 8.0$)	None	No
2	NatureConst-Biased-NoPE	Baseline	Imperfect model ($F = 10.0$ for j=20–24 and $F = 8.0$ elsewhere)	None	No
3	NatureConst-Biased-PE	Baseline	Imperfect model	None	Yes
4	NatureConst-Biased-PE-NoEFSO	Baseline	Imperfect model	None	Yes, but without EFSO
5	NatureVary-Biased-NoPE	Time-varying F	Imperfect model	None	No
6	NatureVary-Biased-PE	Time-varying F	Imperfect model	None	Yes
7	NatureVary-Biased-PE-NoEFSO	Time-varying F	Imperfect model	None	Yes, but without EFSO
8	NatureConst-Biased-ObsBias-PE	Baseline	Imperfect model	Observation bias for j=20–24	Yes

212 Table 1. Summary of the eight cases in this study.

213

214 ## 3. Results and discussion

First, using NatureConst-Perfect-NoPE and NatureConst-Biased-NoPE (Table 1), we investigate the impacts of model bias on the accuracy of DA and the beneficial observation rate. Second, using NatureConst-Biased-PE, we test our proposed approach that uses the beneficial observation rate as a driver of model parameter estimation. Third, using NatureVary-Biased-PE and NatureConst-Biased-ObsBias-PE, we investigate the sensitivity of the new method to experimental settings.

a. Impacts of model bias

As demonstrated in previous studies (e.g., Miyoshi 2005; Kurosawa and Poterjoy 2021), the analysis accuracy of EnKF systems depends on both the covariance inflation coefficient (ρ) and localization scale (σ). Specifically, in NatureConst-Perfect-NoPE in which the model used for LETKF has no bias, root-mean squared errors (RMSEs) become smaller for smaller ρ and larger σ (Figure 1a). In this case, the smallest RMSE is achieved by a combination of $\sigma = 10.0$ and $\rho = 1.02$. In NatureConst-Biased-NoPE in which the model has spatially varying bias (Table 1), the Lorenz96-LETKF system requires a stronger inflation (ρ =1.20) and narrower localization (σ =3.0) to achieve the smallest RMSE (Figure 1b). This combination of ρ and σ is used for calculating the time-mean beneficial observation rate in NatureConst-Biased-NoPE and experiments in Sections 3b and 3c.

The beneficial observation rate is sensitive to model bias. Specifically, when the model used for LETKF has no bias (i.e., NatureConst-Perfect-NoPE), the beneficial observation rate is smaller than 52% in most cases (Figure 1c). In contrast, when the model used for LETKF has spatially varying model bias (i.e., NatureConst-Biased-NoPE), the beneficial observation rate is higher than that in NatureConst-Perfect-NoPE (Figure 1d). The rate is particularly high when LETKF exhibits filter divergence (higher RMSEs), likely because most observations contribute to mitigating model bias.

The beneficial observation rate at each grid point (observation location) clearly depends on whether model bias is present at each grid point. We calculate the time-averaged beneficial observation rate and EFSO impacts at each grid point in the best-performing experiment. The time-averaged beneficial observation rate at the grid points with model bias is clearly higher than that at the other grid points (black curves in Figure 2). In particular, the beneficial observation rate when observations are used as reference states exceeds 56% at the grid points with model bias (blue shaded regions in Figure 2a), whereas the rate at the other grid points is approximately 53%. Similar characteristics are found in the mean EFSO

impacts (magenta curves in Figure 2). The differences in the beneficial observation rate and mean EFSO impacts among the grid points are more evident when observations are used as reference states in EFSO (Figure 2), likely because own analyses are also affected by model bias. In summary, the beneficial observation rate at each grid point clearly depends on whether the model has bias there, indicating that the rate can be used to detect model bias.

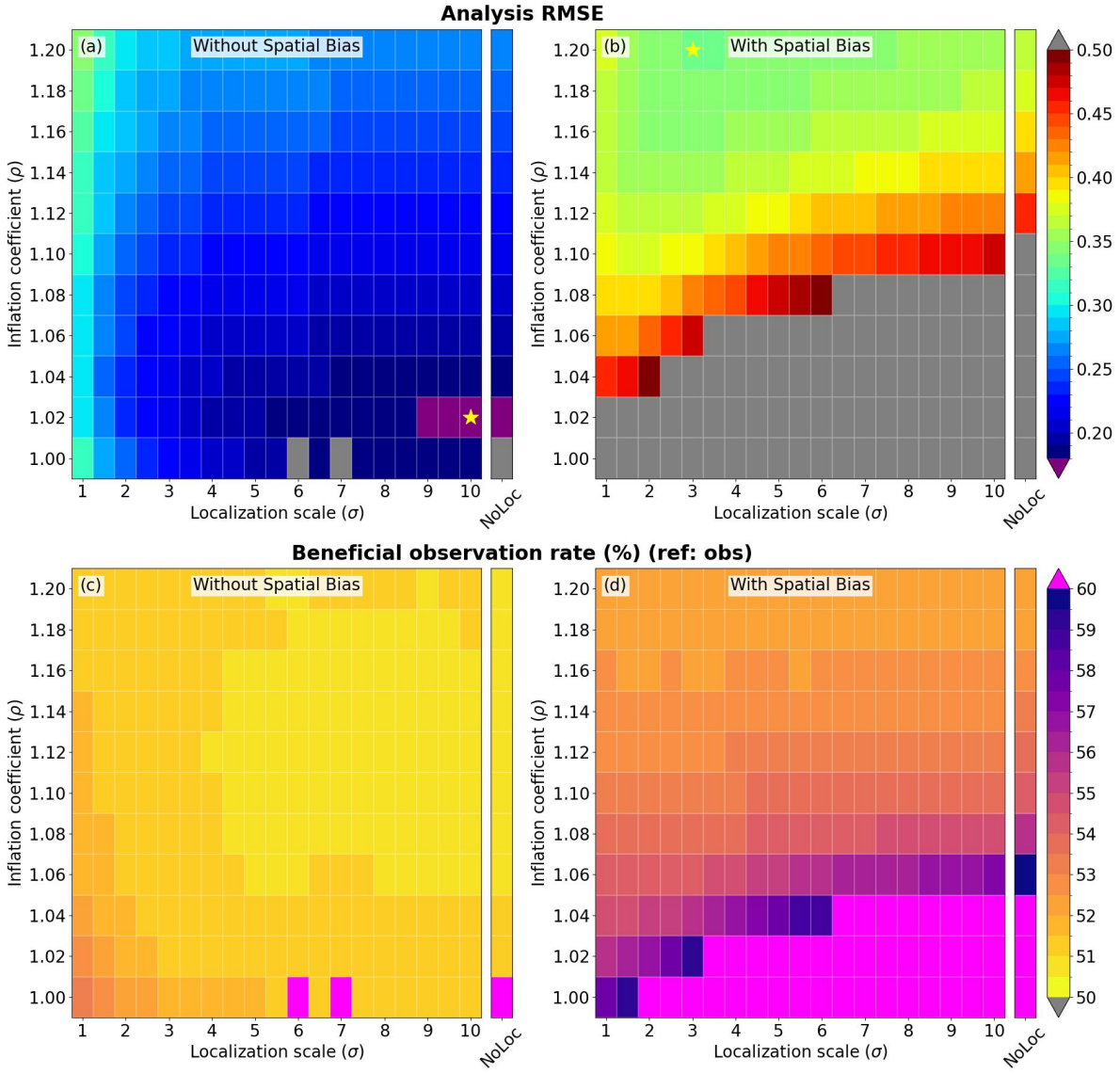

Figure 1: (a), (b) Analysis root-mean-squared errors (RMSEs) and (c), (d) beneficial observation rates (%) diagnosed by EFSO in each experiment. The x and y axes are the localization scale (σ) and covariance inflation coefficient (ρ), respectively. (a) and (c) are NatureConst-Perfect-NoPE in which the model used for LETKF has no bias, whereas (b) and (d) are NatureConst-Biased-NoPE in which the model used for LETKF has model bias. Yellow stars in (a) and (b) indicate the parameter combination that achieved the smallest analysis RMSE. Analysis RMSEs and beneficial observation rates are calculated over 18,000 DA cycles after 2,000 DA cycles for spin-up.

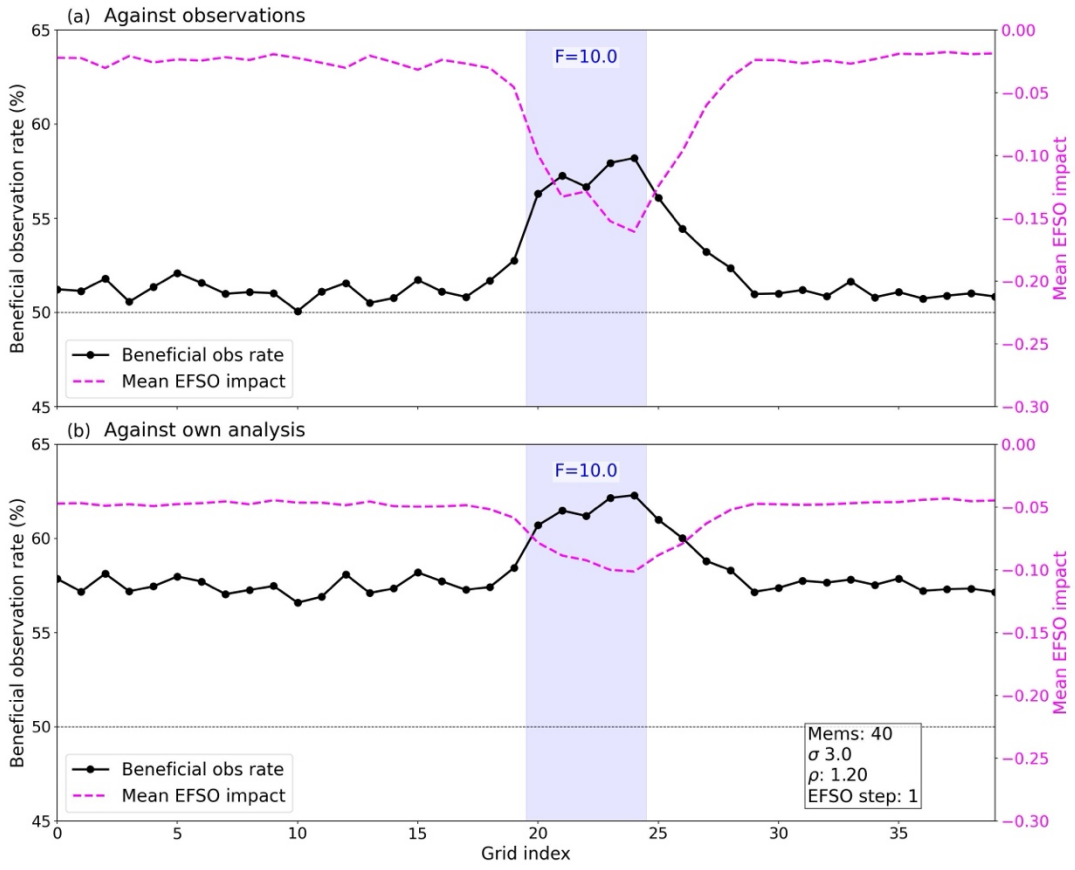

Figure 2: Beneficial observation rate (black curve, %) and time-averaged EFSO impact (dashed magenta curve), based on (a) observations and (b) own analyses as references, at each grid point in NatureConst-Biased-NoPE in which the model used for LETKF has bias at grid points 20–24 (blue shaded regions). The ensemble size, localization scale (σ), inflation coefficient (ρ), and EFSO evaluation time step are 40, 3.0, 1.20, and 1, respectively. The beneficial observation rate and time-averaged EFSO impact are calculated over 18,000 DA cycles after 2,000 DA cycles for spin-up.

b. Parameter estimation using the beneficial observation rate

In this subsection, we test our new approach that uses the beneficial observation rate to trigger model parameter estimation. First, we evaluate the performance of the new approach (NatureConst-Biased-PE) by comparing it with the experiment without parameter estimation (NatureConst-Biased-NoPE) and without using EFSO for parameter estimation (NatureConst-Biased-PE-NoEFSO). Since the beneficial observation rate exceeds 55% at the grid points with model bias (Figure 2a), the threshold value of the beneficial observation rate is set to 55%.

The proposed method successfully detects model bias using the beneficial observation rate and mitigates it through parameter estimation. Specifically, during the first 2,000 DA cycles without parameter estimation, higher beneficial observation rates are found around the

grid points with model bias than at the surrounding grid points (Figure 3a and Figure 3c). In response to these high beneficial observation rates, the new approach introduces ensemble perturbations to the forcing term F (Figure 3b) and model parameter estimation is activated. As a result, the model forcing term F is corrected toward the true value of 8.0 (Figure 3a) and parameter estimation is deactivated (i.e., the ensemble spread of F becomes small (Figure 3b)). Even after F is corrected, parameter estimation is sporadically activated and then quickly deactivated.

The proposed method improves the analysis accuracy as well. By estimating the model parameter, the analysis RMSE with the new approach is lower than that without parameter estimation (Figure 4a). Furthermore, the analysis RMSE with the new approach is lower than that from parameter estimation without EFSO, in the range between 1.01 and 1.06 of inflation coefficient for model parameter tested (Figure 4b). Parameter estimation without EFSO is more sensitive to inflation coefficient for model parameter compared to the new approach. In the new approach, the beneficial observation rate indicates when parameter estimation (i.e., large parameter ensemble spread) is required, so that the new approach is not very sensitive to inflation coefficient for parameter and can exhibit robust performance. Overall, the beneficial observation rate is successfully used to detect model bias and adaptively trigger parameter estimation.

The beneficial observation rate is useful even if the true model parameter varies in time. We test the new approach by comparing NatureVary-Biased-NoPE and NatureVary-Biased-PE, in which the true model parameter at grid points 20–24 oscillates. The beneficial observation rates at these grid points are higher than those at the other grid points (Figure 5a and Figure 5d). As a result, the DA system initiates parameter estimation around these grid points and successfully captures the parameter evolution with a lag (Figure 5b and Figure 5c). Indeed, the analysis RMSE with parameter estimation (i.e., NatureVary-Biased-PE) becomes smaller than that without parameter estimation (i.e., NatureVary-Biased-NoPE) (Figure 4c). Furthermore, the new approach is less sensitive to inflation coefficient of parameter compared to parameter estimation without EFSO (Figure 4d).

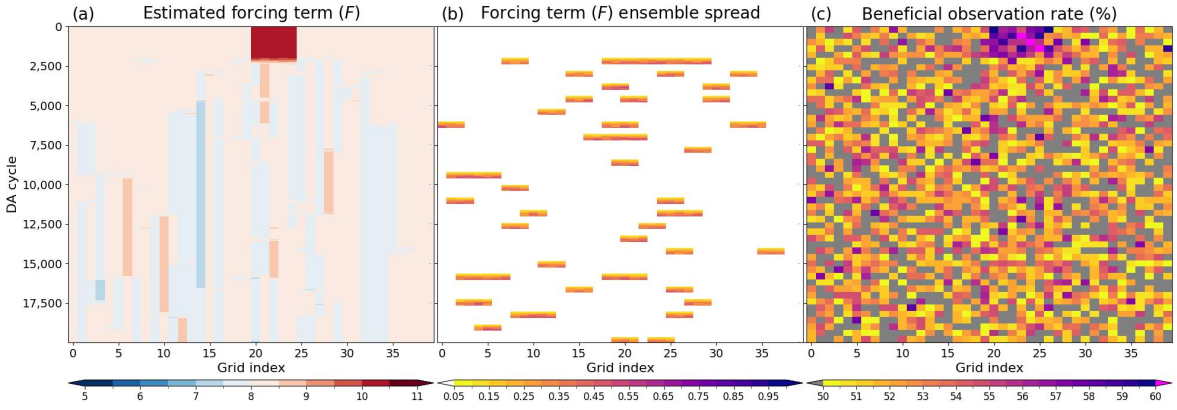

Figure 3: Hovmöller diagrams of (a) the estimated forcing term (F), (b) the ensemble spread of F, and (c) beneficial observation rates (%) in NatureConst-Biased-PE, in which the true forcing term F is globally constant at 8.0 everywhere but the model used for LETKF has bias in F at grid points 20–24. The ensemble size, localization scale (σ), inflation coefficient (ρ), and EFSO evaluation time step are 40, 3.0, 1.20, and 1, respectively.

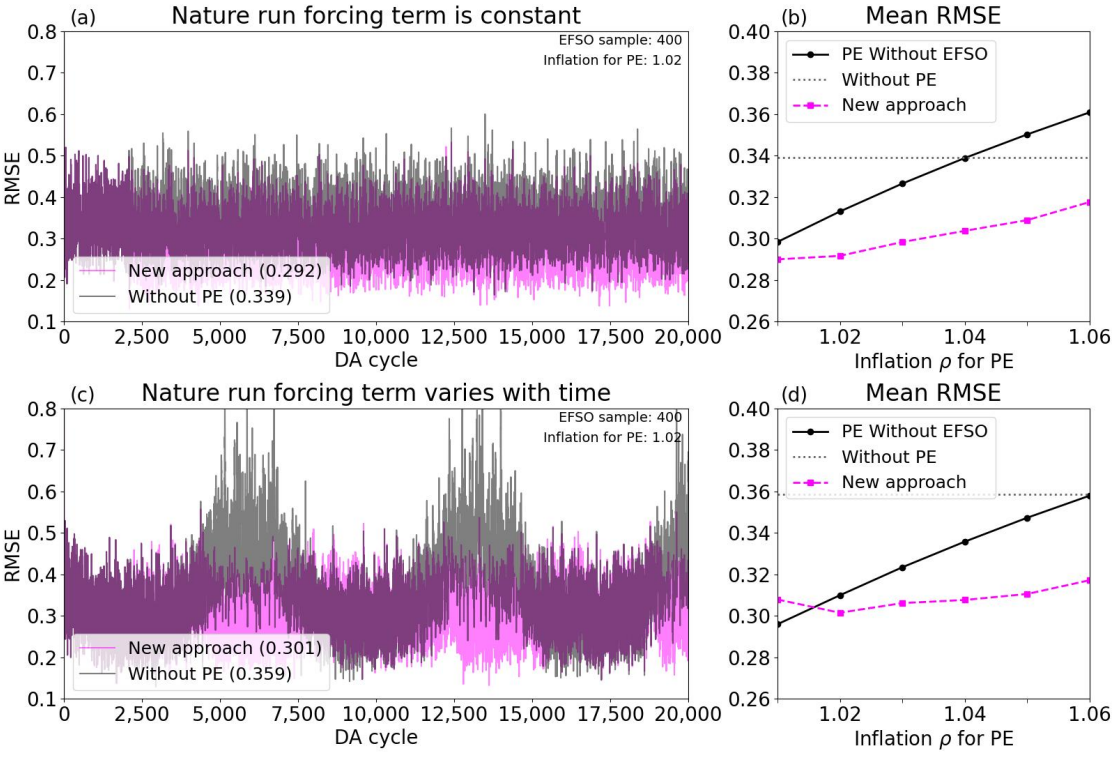

Figure 4: (a), (c) Time series of analysis RMSEs for (a) NatureConst-Biased-NoPE (black) and NatureConst-Biased-PE (magenta), in which the forcing term (F) in the nature run is constant in time, and (c) NatureVary-Biased-NoPE (black) and NatureVary-Biased-PE (magenta), in which F varies in time. Time-averaged analysis RMSEs in each experiment are shown in the legend. (b), (d) Time-averaged analysis RMSEs as a function of inflation coefficient for model parameter for (b) NatureConst-Biased-NoPE (dashed black line), NatureConst-Biased-PE without EFSO (solid black curve), and NatureConst-Biased-PE (solid magenta curve), and for (d) NatureVary-Biased-NoPE (dashed black line), NatureVary-Biased-PE without EFSO (solid black curve), and NatureVary-Biased-PE (magenta curve).

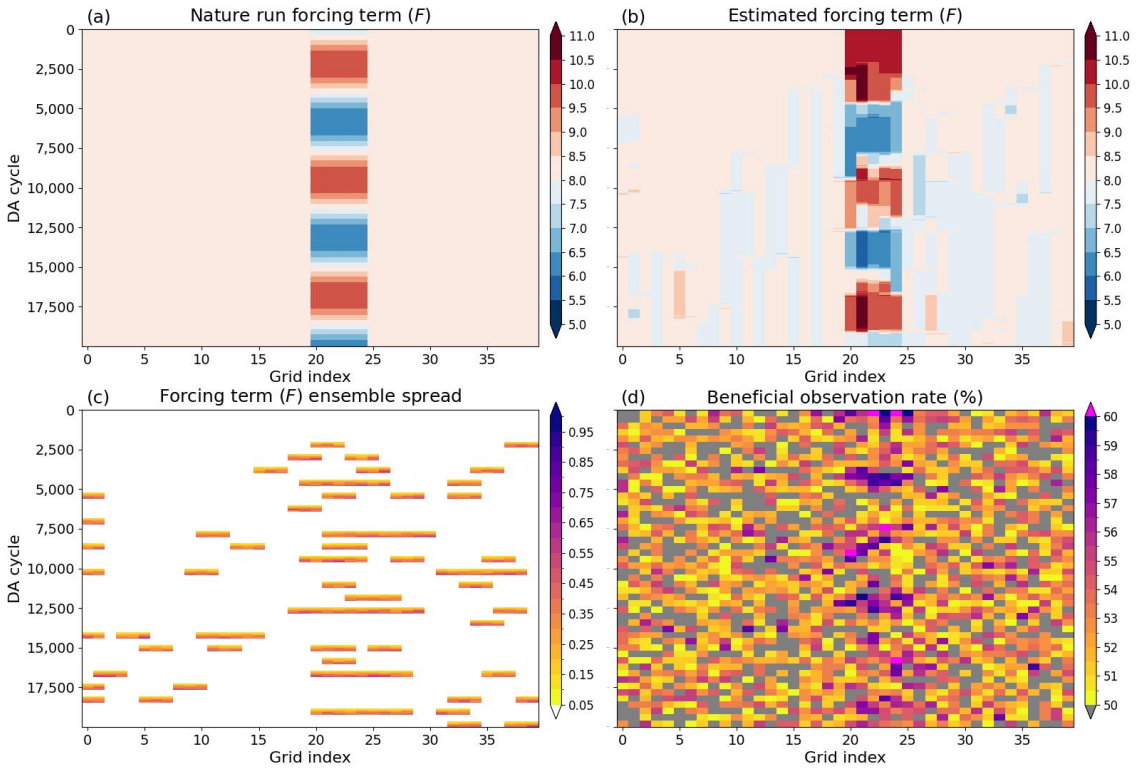

Figure 5: Similar to Figure 3, but showing (a) the true forcing term (F), (b) the estimated forcing term (F), (c) the ensemble spread of the forcing term, and (d) the beneficial observation rate (%) when the true F varies in time (i.e., NatureVary-Biased-PE).

c. Sensitivity to the EFSO verification forecast lead time and observation bias

So far, we have used a fixed EFSO verification forecast lead time of 1 time step; however, previous studies have shown that the beneficial observation rate is sensitive to the verification forecast lead time (e.g., Hotta et al. 2017; Privé et al. 2021). We perform additional experiments with NatureConst-Biased-NoPE and NatureConst-Biased-PE, in which the model used for LETKF has a biased forcing term ($F = 10.0$) at grid points 20–24, with EFSO verification forecast lead times of 5, 10, 15, and 20 time steps and threshold values of the beneficial observation rate of 53%, 55%, 57%, 59%, and 61%.

The beneficial observation rate depends on the EFSO verification forecast lead time. Specifically, the longer the EFSO verification forecast lead time, the lower the beneficial observation rate at the grid points with model bias (Figure 6a). This is consistent with previous studies (Hotta et al. 2017; Privé et al. 2021), which showed that the beneficial observation rate approaches 50% as the FSO verification forecast lead time increases. As a result, to detect model bias and correct it with parameter estimation, our new approach

requires lower threshold values of the beneficial observation rate as the EFSO verification forecast lead time increases (Figure 6b).

The beneficial observation rate can capture model bias even if observations are biased (Figure 7a). We perform additional experiments with NatureConst-Biased-ObsBias-NoPE and NatureConst-Biased-ObsBias-PE, in which observations at grid points 20–24 have biases ranging from –2.0 to 2.0. The results indicate that the beneficial observation rate remains high around the grid points with model bias even if observations are biased. Observation bias often results in a small signal in the time-averaged observation-minus-background, especially when observations have a bias of +0.5, indicating that detecting the bias using the observation-minus-background would be challenging (Figure 7b). Interestingly, even in this case, the beneficial observation rate around the grid points with model bias is clearly higher than that at the other grid points, suggesting that the beneficial observation rate would be useful for detecting model bias.

The improvement in analysis accuracy due to parameter estimation depends on observation bias (Figure 7c). Specifically, the analysis RMSE with positive observation bias is reduced by parameter estimation, whereas the analysis RMSE with negative observation bias is degraded by parameter estimation. The latter is a difficult case, as observation bias partially compensates for model bias. In this case, it would be necessary to simultaneously correct both model and observation biases. Nevertheless, the beneficial observation rate exhibits strong sensitivity to model bias even with observation bias and may provide useful insights into model bias.

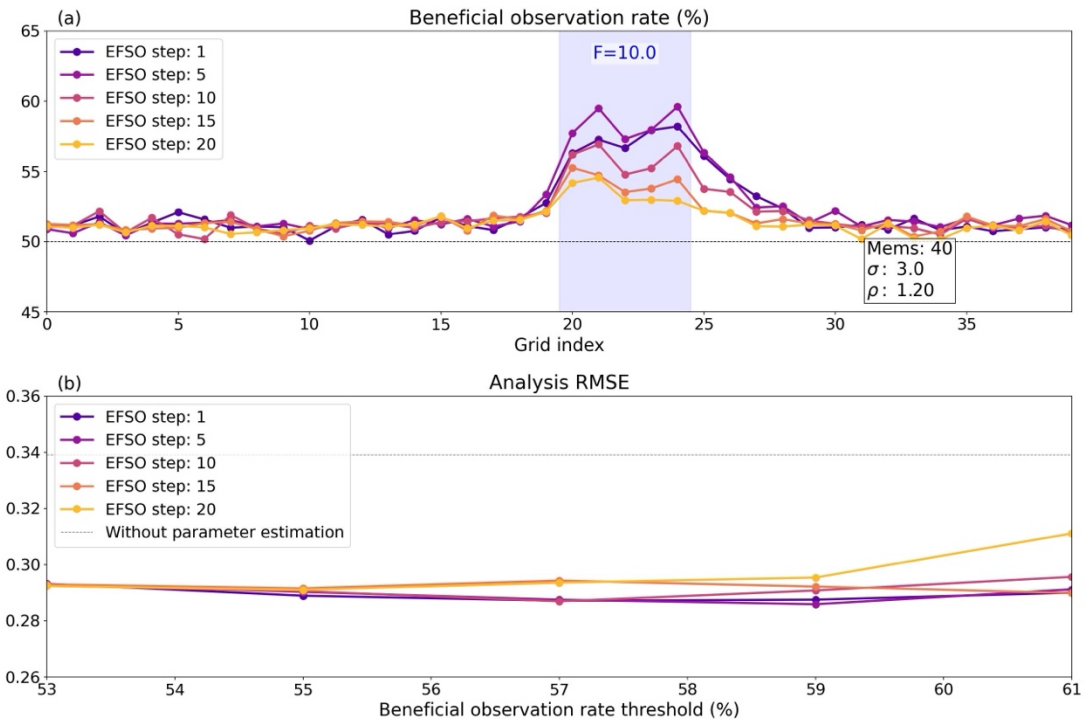

364

365 Figure 6: (a) Similar to Figure 2, but showing the beneficial observation rate (%) for the
366 EFSO verification forecast lead times of 1, 5, 10, 15, and 20 time steps in NatureConst-
367 Biased-PE. (b) Analysis RMSEs without parameter estimation (i.e., NatureConst-Biased-
368 NoPE) (gray) and with parameter estimation (i.e., NatureConst-Biased-PE) based on the
369 EFSO verification forecast lead times of 1, 5, 10, 15, and 20 time steps (warm colors).

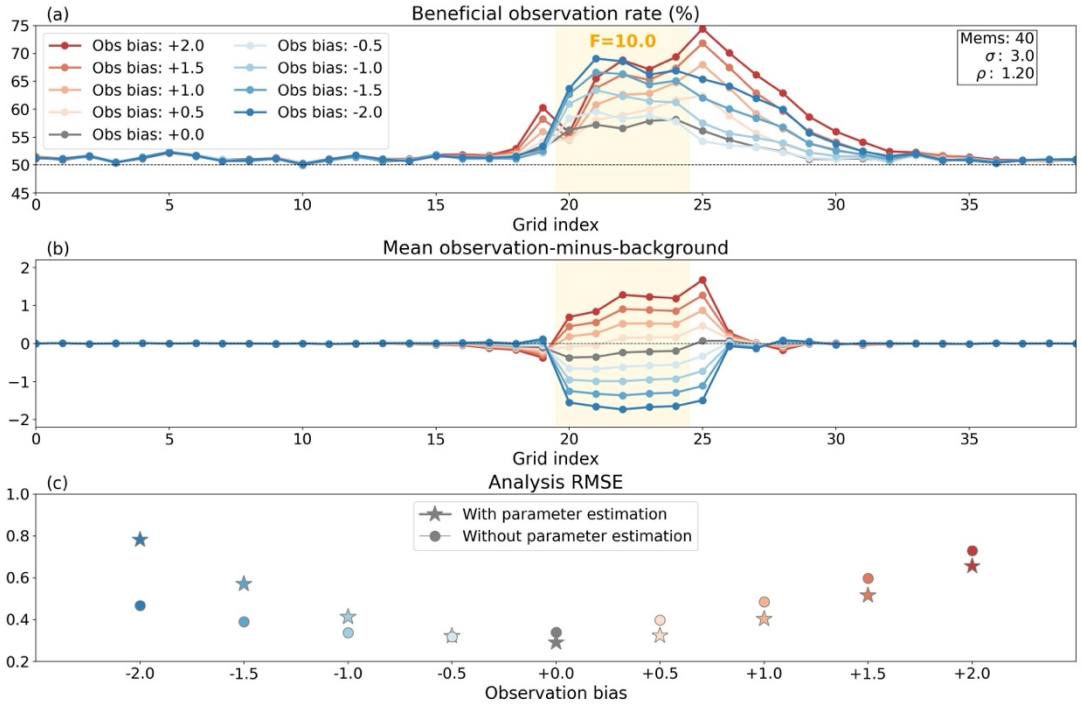

370

371 Figure 7: Similar to Figure 6, but showing (a) the beneficial observation rate in the
372 presence of observation bias at grid points 20–24. Warmer (cooler) colors denote positive

(negative) bias. (b) Analysis RMSE as a function of observation bias at grid points 20–24, with parameter estimation (i.e., NatureConst-Biased-ObsBias-PE) (stars) and without parameter estimation (i.e., NatureConst-Biased-ObsBias-NoPE) (circles).

4. Summary and concluding remarks

In NWP, DA of various observations contributes to improving forecast accuracy. FSO provides useful insights into the contributions of each observing system. Empirically, it is well known that the beneficial observation rate, defined as the proportion of beneficial observations that reduce forecast errors, is approximately 50–60% in practice. Previous studies demonstrated that this rate depends on several factors including model imperfections. The sensitivity of the beneficial observation rate to model bias indicates that the rate may be useful for detecting model bias.

This study proposes using the beneficial observation rate to trigger adaptive parameter estimation. Specifically, parameter estimation is activated around the grid points where the beneficial observation rate exceeds a threshold value. We test this new approach using the Lorenz96 40-variable system with model bias in the forcing term. The results indicate that if the model is biased at several grid points, the beneficial observation rate around these grid points becomes higher than that at the other grid points (Figure 2). By detecting these high beneficial observation rates related to model bias, our new approach successfully activates parameter estimation and improves analysis accuracy (Figure 3 and Figure 4). The new approach also performs well even if the true model parameter (model bias) varies in time and is less sensitive to inflation coefficient for model parameter compared to parameter estimation without EFSO (Figure 4 and Figure 5).

The performance of the new approach depends on several factors such as the verification forecast lead time in FSO, the threshold of the beneficial observation rate, and observation bias. As the verification forecast lead time increases, the beneficial observation rate approaches 50%, consistent with the previous studies, likely due to nonlinear forecast error growth (e.g., Hotta et al. 2017; Privé et al. 2021). In this case, the new approach requires lower threshold values of the beneficial observation rate to detect model bias (Figure 6). Furthermore, the beneficial observation rate may provide useful insights into model bias even if observations are biased. Specifically, when model bias and observation bias are similar, the time-averaged observation-minus-background contains only a weak signal, whereas the beneficial observation rate is clearly high around the grid points with model bias (Figure 7a).

In this case, however, parameter estimation fails to improve analysis accuracy and it would be necessary to simultaneously correct observation bias as well.

In this study, we have investigated the characteristics of the beneficial observation rate, its potential to detect model bias, and its use as a trigger for parameter estimation using the Lorenz96 40-variable model. In future research, it would be necessary to test the new approach with more realistic models and observations. Furthermore, it would be interesting to incorporate the beneficial observation rate into advanced model parameter estimation methods (Sawada 2022; Sawada and Duc 2024).

Acknowledgments.

TH was partially supported by JSPS KAKENHI (JP24K07127). YS was partially supported by JST Moonshot R&D program (Grant JMPJMS2281) and JSPS KAKENHI JP25H00760, JP26K00012).

Data Availability Statement.

The source code of the Lorenz96-40 system and analysis scripts used in this study are archived at Zenodo (https://zenodo.org/records/19837678). The archived version corresponds to the code used in this study.

REFERENCES

Aksoy, A., F. Zhang, and J. W. Nielsen-Gammon, 2006a: Ensemble-based simultaneous state and parameter estimation with MM5. *Geophys. Res. Lett.*, **33**, 2951–2970.

Aksoy, A., F. Zhang, and J. W. Nielsen-Gammon, 2006b: Ensemble-based simultaneous state and parameter estimation in a two-dimensional Sea-Breeze model. *Mon. Weather Rev.*, **134**, 2951–2970.

Anderson, J. L., 2001: An ensemble adjustment Kalman filter for data assimilation. *Mon. Weather Rev.*, **129**, 2884–2903.

Bormann, N., H. Lawrence, and J. Farnan, 2019: Global observing system experiments in the ECMWF assimilation system.

Chen, T. C., and E. Kalnay, 2019: Proactive quality control: Observing system simulation experiments with the Lorenz ’96 model. *Mon. Weather Rev.*, **147**, 53–67.

—, and ——, 2020: Proactive quality control: observing system experiments using the NCEP global forecast system. *Mon. Weather Rev.*, **148**, 3911–3931.

Dahoui, M., L. Isaksen, and G. Radnoti, 2017: Assessing the impact of observations using observation-minus-forecast residuals. *ECMWF*. Accessed March 12, 2026, https://www.ecmwf.int/en/newsletter/152/meteorology/assessing-impact-observations-using-observation-minus-forecast.

Evensen, G., 1994: Sequential data assimilation with a nonlinear quasi-geostrophic model using Monte Carlo methods to forecast error statistics. *J. Geophys. Res.*, **99**, 10143–10162.

Gaspari, G., and S. E. Cohn, 1999: Construction of correlation functions in two and three dimensions. *Quart. J. Roy. Meteor. Soc.*, **125**, 723–757.

Gasperoni, N. A., X. Wang, K. A. Brewster, and F. H. Carr, 2024: Exploring Ensemble Forecast Sensitivity to Observations for a Convective-Scale Data Assimilation System over the Dallas–Fort Worth Testbed. *Mon. Weather Rev.*, **152**, 571–588.

Honda, T., and A. Yamazaki, 2024: Machine Learning Enables Real-Time Proactive Quality Control: A Proof-Of-Concept Study. *Geophys. Res. Lett.*, **51**, https://doi.org/10.1029/2023GL107938.

—, ——, and K. Okamoto, 2026: Ensemble forecast sensitivity to observations (EFSO) applied to all-sky infrared radiance observations. *Mon. Weather Rev.*, **1**, https://doi.org/10.1175/mwr-d-25-0248.1.

Hotta, D., T. C. Chen, E. Kalnay, Y. Ota, and T. Miyoshi, 2017: Proactive QC: A fully flow-dependent quality control scheme based on EFSO. *Mon. Weather Rev.*, **145**, 3331–3354.

Houtekamer, P. L., and F. Zhang, 2016: Review of the ensemble Kalman filter for atmospheric data assimilation. *Mon. Weather Rev.*, **144**, 4489–4532.

Hunt, B. R., E. J. Kostelich, and I. Szunyogh, 2007: Efficient data assimilation for spatiotemporal chaos: A local ensemble transform Kalman filter. *Physica D*, **230**, 112–126.

Ishibashi, T., 2018: Adjoint-based observation impact estimation with direct verification using forward calculation. *Mon. Weather Rev.*, **146**, 2837–2858.

Jung, Y., M. Xue, and G. Zhang, 2010: Simultaneous estimation of microphysical parameters and the atmospheric state using simulated polarimetric radar data and an ensemble Kalman filter in the presence of an observation operator error. *Mon. Weather Rev.*, **138**, 539–562.

Kalnay, E., Y. Ota, T. Miyoshi, and J. Liu, 2012: A simpler formulation of forecast sensitivity to observations: application to ensemble Kalman filters. *Tellus A*, **64**, 18462–18462.

Kotsuki, S., S. J. Greybush, and T. Miyoshi, 2017: Can we optimize the assimilation order in the serial ensemble Kalman filter? A study with the Lorenz-96 model. *Mon. Weather Rev.*, **145**, 4977–4995.

—, K. Terasaki, H. Yashiro, H. Tomita, M. Satoh, and T. Miyoshi, 2018: Online Model Parameter Estimation With Ensemble Data Assimilation in the Real Global Atmosphere: A Case With the Nonhydrostatic Icosahedral Atmospheric Model (NICAM) and the Global Satellite Mapping of Precipitation Data. *Journal of Geophysical Research: Atmospheres*, **123**, 7375–7392.

—, K. Kurosawa, and T. Miyoshi, 2019: On the properties of ensemble forecast sensitivity to observations. *Quart. J. Roy. Meteor. Soc.*, **145**, 1897–1914.

—, Y. Sato, and T. Miyoshi, 2020: Data Assimilation for Climate Research: Model Parameter Estimation of Large-Scale Condensation Scheme. *Journal of Geophysical Research: Atmospheres*, **125**, https://doi.org/10.1029/2019JD031304.

Kurosawa, K., and J. Poterjoy, 2021: Data Assimilation Challenges Posed by Nonlinear Operators: A Comparative Study of Ensemble and Variational Filters and Smoothers. *Mon. Weather Rev.*, **149**, 2369–2389.

Langland, R. H., and N. L. Baker, 2004: Estimation of observation impact using the NRL atmospheric variational data assimilation adjoint system. *Tellus A*, **56**, 189–189.

Lorenc, A. C., and R. T. Marriott, 2014: Forecast sensitivity to observations in the Met Office Global numerical weather prediction system. *Quart. J. Roy. Meteor. Soc.*, **140**, 209–224.

Lorenz, E. N., and K. A. Emanuel, 1998: Optimal sites for supplementary weather observations: Simulation with a small model. *J. Atmos. Sci.*, **55**, 399–414.

Miyoshi, T., 2005: Ensemble Kalman Filter Experiments With a Primitive-Equation Global Model. *Ph.D. dissertation, University of Maryland, College Park*, 197–197.

—, and S. Yamane, 2007: Local ensemble transform Kalman filtering with an AGCM at a T159/L48 resolution. *Mon. Weather Rev.*, **135**, 3841–3861.

—, ——, and T. Enomoto, 2007: Localizing the Error Covariance by Physical Distances within a Local Ensemble Transform Kalman Filter (LETKF). *SOLA*, **3**, 89–92.

Necker, T., M. Weissmann, and M. Sommer, 2018: The importance of appropriate verification metrics for the assessment of observation impact in a convection-permitting modelling system. *Quart. J. Roy. Meteor. Soc.*, **144**, 1667–1680.

Nystrom, R. G., S. J. Greybush, X. Chen, and F. Zhang, 2021: Potential for new constraints on tropical cyclone surface-exchange coefficients through simultaneous ensemble-based state and parameter estimation. *Mon. Weather Rev.*, **149**, 2213–2230.

508 —, C. Snyder, and M. El Gharamti, 2023: A One-Step-Ahead Ensemble Kalman Smoothing
509 Approach Toward Estimating the Tropical Cyclone Surface-Exchange Coefficients.
510 *Mon. Weather Rev.*, **151**, 625–642.

511 Ota, Y., J. C. Derber, E. Kalnay, and T. Miyoshi, 2013: Ensemble-based observation impact
512 estimates using the NCEP GFS. *Tellus A*, **65**, 20038–20038.

513 Privé, N. C., R. M. Errico, R. Todling, and A. El Akkraoui, 2021: Evaluation of adjoint-based
514 observation impacts as a function of forecast length using an Observing System
515 Simulation Experiment. *Quart. J. Roy. Meteor. Soc.*, **147**, 121–138.

516 Ruiz, J. J., M. Pulido, and T. Miyoshi, 2013a: Estimating model parameters with ensemble-
517 based data assimilation: A review. *J. Meteorol. Soc. Japan*, **91**, 79–99.

518 —, ——, and ——, 2013b: Estimating model parameters with ensemble-based data
519 assimilation: Parameter covariance treatment. *J. Meteorol. Soc. Japan*, **91**, 453–469.

520 Samrat, N. H., and Coauthors, 2025: Observation impact evaluation through data denial
521 experiments in the Met Office global numerical weather prediction system. *Quart. J.*
522 *Roy. Meteor. Soc.*, **151**, 1–21.

523 Sawada, Y., 2022: An efficient estimation of time‐varying parameters of dynamic models
524 by combining offline batch optimization and online data assimilation. *J. Adv. Model.*
525 *Earth Syst.*, **14**, https://doi.org/10.1029/2021ms002882.

526 —, and L. Duc, 2024: An Efficient and Robust Estimation of Spatio-Temporally Distributed
527 Parameters in Dynamic Models by an Ensemble Kalman Filter. *J. Adv. Model. Earth*
528 *Syst.*, **16**, https://doi.org/10.1029/2023MS003821.

529 Schirber, S., D. Klocke, R. Pincus, J. Quaas, and J. L. Anderson, 2013: Parameter estimation
530 using data assimilation in an atmospheric general circulation model: From a perfect
531 toward the real world. *J. Adv. Model. Earth Syst.*, **5**, 58–70.

532 Sommer, M., and M. Weissmann, 2014: Observation impact in a convective-scale localized
533 ensemble transform Kalman filter. *Quart. J. Roy. Meteor. Soc.*, **140**, 2672–2679.

534 —, and ——, 2016: Ensemble-based approximation of observation impact using an
535 observation-based verification metric. *Tellus A*, **68**,
536 https://doi.org/10.3402/tellusa.v68.27885.

537 Sueki, K., S. Nishizawa, T. Yamaura, and H. Tomita, 2022: Precision and convergence speed
538 of the ensemble Kalman filter-based parameter estimation: setting parameter
539 uncertainty for reliable and efficient estimation. *Prog. Earth Planet. Sci.*, **9**,
540 https://doi.org/10.1186/s40645-022-00504-4.

541 Tomizawa, F., and Y. Sawada, 2021: Combining ensemble Kalman filter and reservoir
542 computing to predict spatiotemporal chaotic systems from imperfect observations and
543 models. *Geosci. Model Dev.*, **14**, 5623–5635.

544 Yamazaki, A., T. Miyoshi, J. Inoue, T. Enomoto, and N. Komori, 2021: EFSO at different
545 geographical locations verified with observing system experiments. *Weather*
546 *Forecast.*, **36**, 1219–1236.

547 —, K. Terasaki, T. Miyoshi, and S. Noguchi, 2023: Estimation of AMSU-A Radiance
548 Observation Impacts in an LETKF-Based Atmospheric Global Data Assimilation
549 System: Comparison with EFSO and Observing System Experiments. *Weather*
550 *Forecast.*, **38**, 953–970.